J. C. Wyant

C. L. Koliopoulos

Optical Sciences Center,
University of Arizona,
Tucson, Ariz. 85721

B. Bhushan

GPD Laboratory,
IBM Corporation,
Tucson, Ariz. 85744
Fellow ASME

D. Basila

WYKO Corporation,
2990 E. Fort Lowell
Tucson, Ariz. 85716

Development of a Three-Dimensional Noncontact Digital Optical Profiler

A noncontact three-dimensional optical profiler for measuring surface roughness is described. The system consists of a reflection microscope, Mirau interferometer with a reference surface mounted on a piezoelectric transducer, CID detector array, frame grabber, and micro-computer. Interferometric phase-shifting techniques are used to obtain surface height information. The height measurements areprocessed by a computer to obtain topographical statistical parameters, which are useful in predicting tribological and magnetic performances of the head-media interface in magnetic storage systems. Sample data are presented for magnetic media (tape, floppy disk, and rigid disk), a magnetic head, a silicon wafer, *and a glass slide.*

1 Introduction

Surface roughness plays a significant role in the performance of precision machines. Roughness is typically measured by a stylus instrument that amplifies and records the vertical motions of a stylus as it moves at a constant velocity across the surface to be measured. For soft surfaces, however, noncontacting techniques such as optical methods are preferable [l, 2]. Besides, commercially available techniques provide only two-dimensional profiles. For a complete surface characterization, it is necessary to have a quantitative, three-dimensional assessment of the surface asperities.

Various attempts at obtaining three-dimensional measurements of surface asperities have been reported in the literature [3-11] Resolution limitations of several techniques are presented in Table 1. Resolutions of the instruments reported in references [3] through [7] are not adequate, and some instruments require immovable large equipment. The technique of reference [8] uses a conventional stylus profile meter and a precision table that moves perpendicularly to the tracing direction of the stylus. The disadvantage of this technique is that it cannot reference two consecutive traces. Scanning tunnelling microscopy [9-ll] can provide topographic information on the atomic scale; however, considerable hardware development is needed before this technique can be used commercially.

Recently, we reported a noncontact technique for measuring two-dimensional surface roughness using a Mirau interferometer [1, 2]. An electronic phase-measurement technique was used with a linear, solid-state, detector array to provide digital profile data. Using a two-dimensional solid-state detector array, we have developed a three-dimensional profiler. The instrument is automated. Extensive software has been developed to provide complete surface topographical statistics. This paper presents details of the instrument's hardware and software, and typical results.

Table 1 Resolutions of different surface roughness measurement techniques

Type	Contact or noncontact	Resolution	
		Lateral	Vertical
Stylus	Contact	1-2 μm	5 nm
Optical	Noncontact	1 μm	0.5-l nm
SEM stereoscopy	Noncontact	2-4 nm	l0-20 nm
Tunnelling microscopy	Noncontact	0.3 nm	0.02 nm

2 The Optical Profiler

Figure 1 is a schematic of the three-dimensional digital optical profiler. The light source is a tungsten halogen bulb. A spectral filter of 40-nm bandwidth, centered at a wavelength of 650 nm, reduces the spectral bandwidth of the source and increases its coherence length. The profiler uses a two-beam Mirau interferometer. The reference surface in the interferometer is mounted on a piezoelectric transducer (PZT), so that during measurements a voltage can be applied to the PZT to move it at a constant velocity. This allows the use of electronic phase-shifting techniques to measure the phase of the interference pattern as described below. The profiler works with 10X and 20X magnification objectives. The interference fringe pattern is seen by looking through the eyepieces. The fringes illuminate a 384 x 244 pixel charge-injection-device (CID) image sensor with pixel spacing of approximately 25 μm square. In data analysis, a 224 x 224 pixel portion of the array is used. When the 10X objective is used, the pixel spacing on the surface being measured is about 2.5 μm and the total area being measured is 0.56 x 0.56 mm. With the 20X objective, the pixel spacing is about 1.25 μm and the measured area is 0.28 x 0.28 mm.

Contributed by the Tribology Division of THE AMERICAN SOCIETY OF MECHANICAL ENGINEERS and presented at the ASME/ASLE Joint Tribology Conference, Atlanta, Ga., October 8-10, 1985. Manuscript received by the Tribology Division May 1, 1985. Paper No. 85-Trib-15.

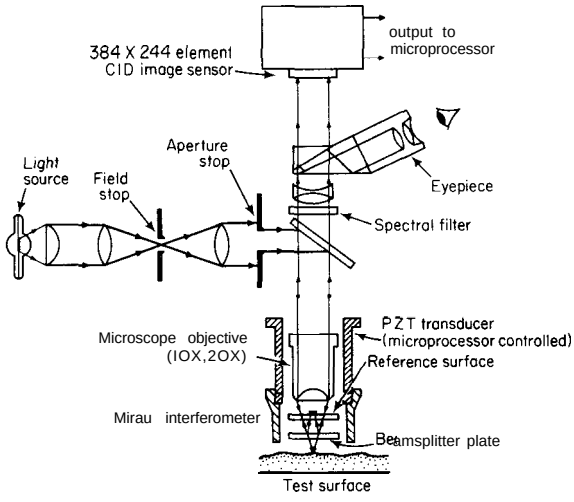

Fig. 1 Schematic of the three-dimensional digital optical profiler

Figure 2(a) is a photograph of the complete profiler hardware. Figure 2(b) is a block diagram of the entire system. The CID image sensor is used at standard video-field rates of l/60 second per image of 384 pixels by 244 lines. The motion of the PZT is synchronized with the horizontal line rate of the image sensor. The analog video signal from the image sensor is digitized by a video frame grabber, modified so that all four consecutive images of 384 x 244 pixels can be acquired. These frames are digitized to 8 bits per detector element in l/15 s. The result is stored in digital memory as four images of the interference pattern, each integrated over different 90-degree phase shifts of the fringes.

Acquisition of the video signal, digitization, and the motion of the piezoelectric transducer are controlled by a microcomputer. The microcomputer tests the video horizontal blanking status of the video from the frame grabber electronics and changes the position of the PZT by sending a value to a 12-bit digital-to-analog (D/A) converter. This analog voltage is amplified to drive the PZT, which has a sensitivity of about 500 V per micrometer of displacement.

Once the four interference images are digitized and placed in the frame grabber's memory, the microcomputer calculates the phase at each detector element, as described below. This phase is proportional to the surface height at that location. Further calculations produce a two-dimensional array of height elements of the surface under test over a 224 x 224 pixel array. This information can be displayed in a gray-scale representation on a video display, where 256 gray values represent the surface heights in the image. The array of height values is transferred to a desktop computer via an HPIB interface. This computer provides the software programs that further analyze the surface height data and can display the results with color graphics or various two- and three-dimensional plots, as described in Section 3.

2.1 Phase Measurement. Several phase-measurement techniques can be used in an optical profiler to give more accurate height measurements than is possible by simply using the traditional technique of looking at the interference fringes and determining how much they depart from being straight and equally spaced. The profiler described in this paper uses the so-called integrated bucket technique. Because this technique has been described in detail in reference [2], it is summarized only briefly here.

For the integrated bucket technique, the phase difference, α, between the two interfering beams is changed at a constant rate, *t*, as the detector is read out. During each time the detector array is read out, the phase, Ø(x,y), has changed by 90 deg for each pixel. The basic equation for the intensity of a two-beam interference pattern is given by

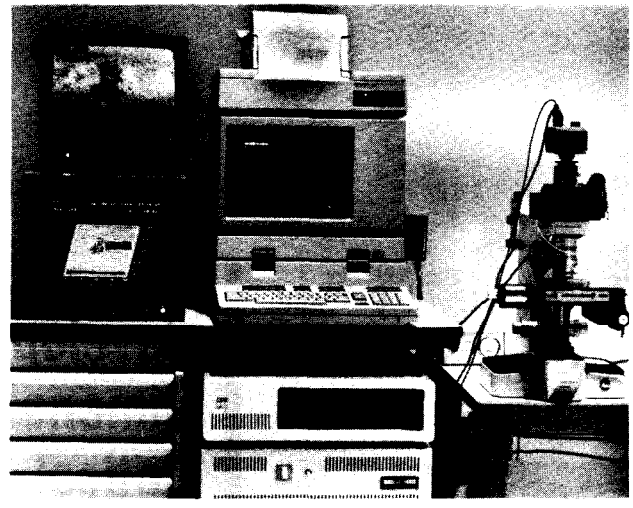

Fig. 2(a)

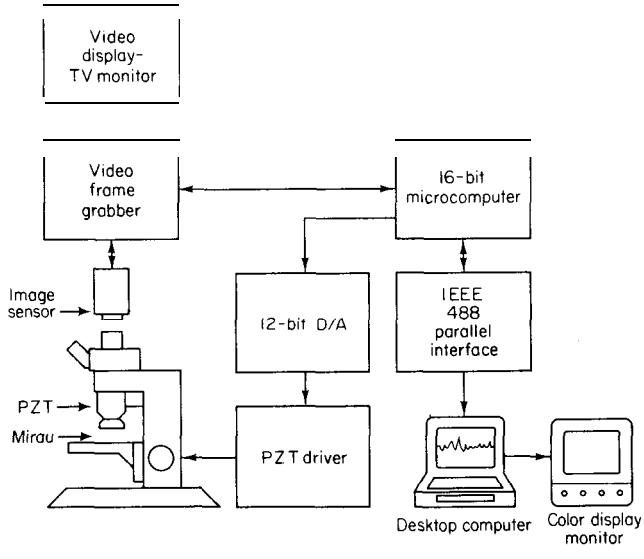

Fig. *2(b)*

Fig. 2 Photograph (a) and block diagram (b) **of the instrumentation and processing system**

$$I = I_1 + I_2 \cos[\phi(x,y) + \alpha(t)], \tag{1}$$

where the first term is the average intensity and the second term is the interference term. If the intensity is integrated while o(t) varies from 0 to $\pi/2$, $\pi/2$ to π, and π to $3\pi/2$, the resulting signals are given by

$$\begin{aligned} A(x,y) &= I_1' + I_2'[\cos\phi(x,y) - \sin\phi(x,y)] \\ B(x,y) &= I_1' + I_2'[-\cos\phi(x,y) - \sin\phi(x,y)] \\ C(x,y) &= I_1' + I_2[-\cos\phi(x,y) + \sin\phi(x,y)] \end{aligned} \tag{2}$$

From the values of A, B, and C, the phase can be calculated as

$$\phi(x,y) = \tan^{-1}[(C(x,y) - B(x,y))/(A(x,y) - B(x,y))]. \tag{3}$$

This phase measurement is performed at each detector point. The subtraction and division cancel out the effects of fixed-pattern noise and gain variations across the detector, as long as the effects are not so large as to make the dynamic range of the detector too small to be of use.

For the profiler data described in this paper, four frames of intensity data were measured. The phase Ø(x,y) was first calculated, by means of equation (3), using the first three of the four frames. It was then similarly calculated using the last three of the four frames. These two calculated phase values

were then averaged to increase the accuracy of the measurement.

Because equation (3) gives the phase modulo 2π, there may be 2π discontinuities present in the calculated phase. These 2π discontinuities can be removed as long as the slopes on the sample being measured are limited so that the actual phase difference between adjacent pixels is less than π. Removal of the 2π discontinuities is done by checking the phase difference between adjacent pixels and, whenever the difference is greater than π, either adding or subtracting a multiple of 2π to reduce the phase difference to less than π.

Once the phase $\phi(x,y)$ is determined across the interference field, the corresponding height distribution $h(x,y)$ is determined by the equation

$$h(x,y) = (\lambda/4\pi)\phi(x,y). \quad (4)$$

3 Data Analysis

The measured height distribution across the sample can be analyzed to determine many properties about the sample. The following surface topography statistics are given by the system: surface-height distributions; surface slope and curvature distributions in x, y, and radial directions; all peaks and upper 25 percent peak heights, absolute slopes, and curvatures; peak density and upper 25 percent peak density; number of zero crossings per unit length in x, y, and two dimensions; and three-dimensional plot of autocovariance function with a contour of autocovariance function at 0 and 0.1. In addition to the plots, color and gray level contour maps are available for surface height variations; surface slope and curvature variations in x, y, and radial directions; and autocovariance of the surface height variations. The importance of the measured statistical parameters in studying the tribology of sliding surfaces has been discussed in detail in reference [2].

3.1 Surface Heights.

Three-Dimensional Plots. The height variations across the sample are fitted in a least squares sense to determine the average height, the tilt, and the curvature. The average height is always subtracted, and usually the tilt is also subtracted. The curvature is also usually removed when magnetic tape or floppy disks are measured because the curvature is a result of the sample's not being flat. The peak-valley distance (P-V) is determined by finding the difference between the maximum and minimum height values. The root mean square (rms) of the height distribution is also calculated.

Profile. Surface profiles are plotted in the x and y directions across the center of the sample being measured. Other profile plots in both directions can also be obtained.

Histogram. To calculate the histogram of surface heights, the data are grouped into 50 bins. From the rms surface height and the fact that the average height is zero, it is possible to plot the Gaussian height distribution for the data.

Probability Paper Plots. The surface height data are plotted on probability paper to show the percentage of the surface heights below a given height. A straight line corresponding to a normal distribution is drawn on the plot. The slope of the straight line portion is determined by the rms surface height, and the position of the line for 50 percent probability is set at the average height value, zero.

3.2 Profile and Surface Slopes. The profile slopes in the x and y directions are obtained by finding the height difference between adjacent detector pixels. The surface slope is obtained by finding the square root of the sum of the squares of the x and y slopes at each point [12]. Histograms and probability plots are drawn for profile slopes in the x and y axes and for surface slope. The rms and P-V values are also calculated.

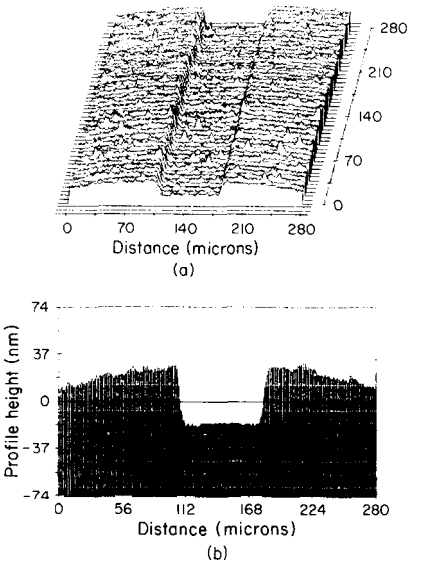

Fig. 3 Plots of a calibration standard. *(a)* Surface plot. *(b)* Profile in the x axis.

3.3 Profile and Surface Curvatures. The profile curvatures in the x and y directions are obtained by finding the difference between the slopes calculated at adjacent pixels. The surface curvature is calculated by the average of the x and y curvatures [12]. Histograms and probability plots are drawn for profile curvatures in the x and y axes and for surface curvature. The rms and P-V values are also calculated.

3.4 Autocovariance Plots. A 128 x 128 pixel portion of the data from the center of the data set is used to determine the autocovariance of the surface height data. The autocovariance is calculated by taking a Fast Fourier Transform (FFT) of the surface-height data, squaring the results, and then taking another FFT. A three-dimensional plot is drawn. Two-dimensional plots are drawn showing the points for which the autocovariance is greater than zero and the points for which the autocovariance is greater than 0.1 of the maximum value. For the latter plot, the minimum, maximum, and mean distances for which the autocovariance drops to 0.1 of the maximum are calculated. The anisotropy ratio, defined as the ratio of maximum to minimum distance, is also calculated. The autocorrelation distance represents a degree of randomness; therefore, the loci of points where the autocovariance function is greater than 0.1 of the maximum value would be a circle if the anisotropy ratio were 1.

Profile slices through the autocovariance function for 0, 90, and ± 45 deg are drawn.

3.5 Summits. A summit is defined as a point higher than its four adjacent points. To eliminate the effects of noise and ensure that every peak identified is truly substantial, we required further that it be at least 2.2 nm above the four nearest points.

The curvature of a summit is calculated by looking at the slope between the summit and the points on each side of it in the x and y directions. Summit curvature is the mean of curvatures between the x and y directions [12]. The absolute slopes between a summit and adjacent valleys in the ±x and ±y directions are also calculated. A valley is defined as points at least 2.2 nm below the two adjacent points in the x direction for x slopes and in the y direction for y slopes. The absolute slope in the x and y directions is calculated by taking the mean of the absolute slopes on positive and negative sides in the x and y directions, respectively. The summit absolute slope is

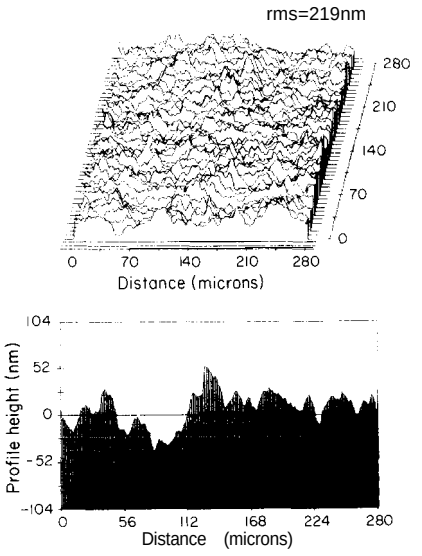

Fig. *4(a)*

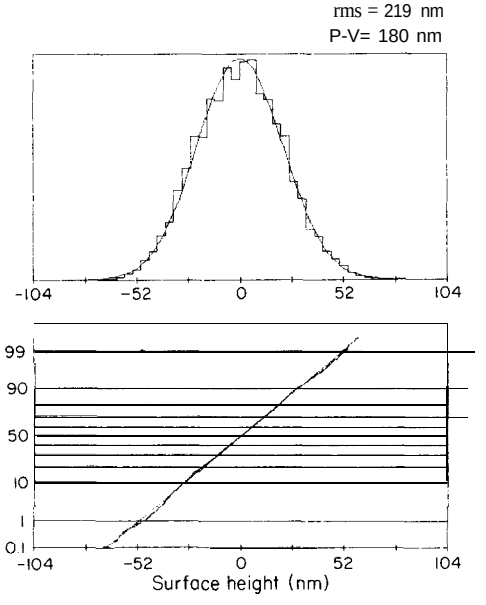

Fig. *4(b)*

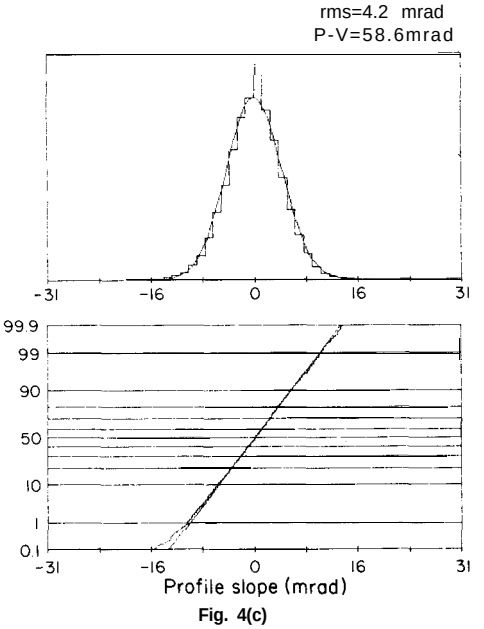

Fig. 4(c)

calculated by taking the mean of absolute slopes in the x and y directions.

The mean, maximum, minimum, and standard deviation for summit height, curvature, radius (l/curvature), and the absolute slope are calculated for all summits and for those summits having a height within the upper 25 percent of the maximum summit. (Upper 25 percent peaks reported for the two-dimensional profiler [l, 2] were 25 percent of the highest peaks.) Histograms and probability plots were made for heights of surface summits, slopes of the summits, and curvature of the summits. Corresponding plots were made for the data obtained using the upper 25 percent of the highest summits. The number of summits per square millimeter was also measured.

The number of times per millimeter that the profile passed through zero in the x direction and in the y direction was measured. The number of times per millimeter that the surface passed through zero was calculated. To calculate the

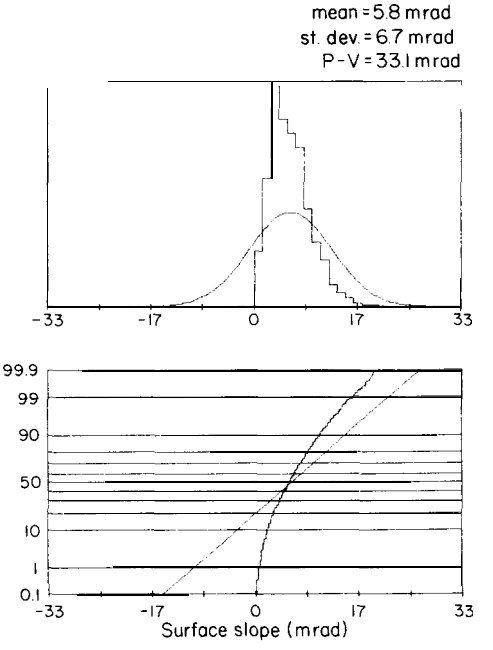

Fig. 4(d)

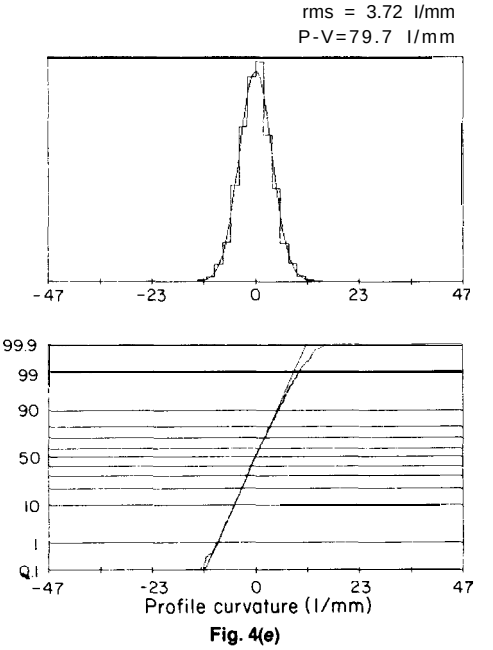

Fig. 4(e)

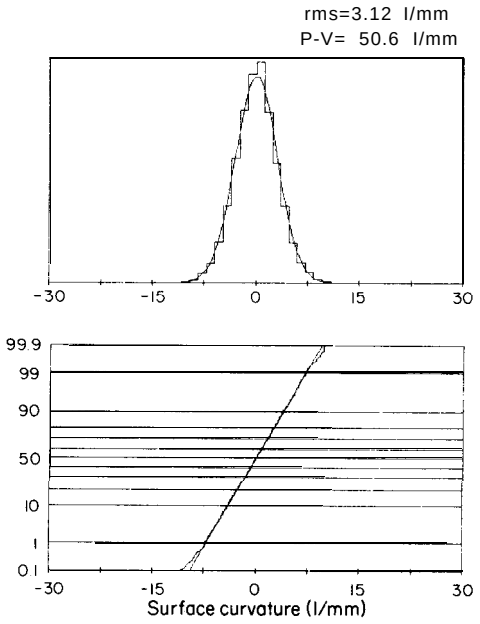

Fig. 4(*f*)

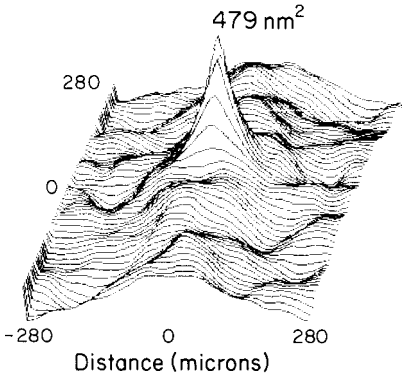

Fig. 4(*g*)

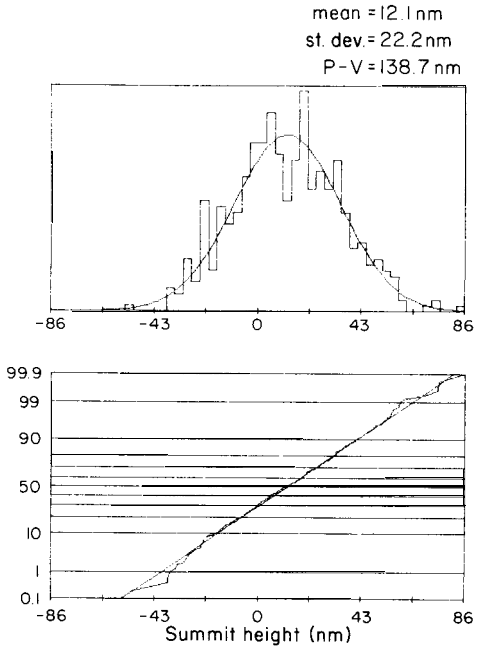

Fig. 4(*h*)

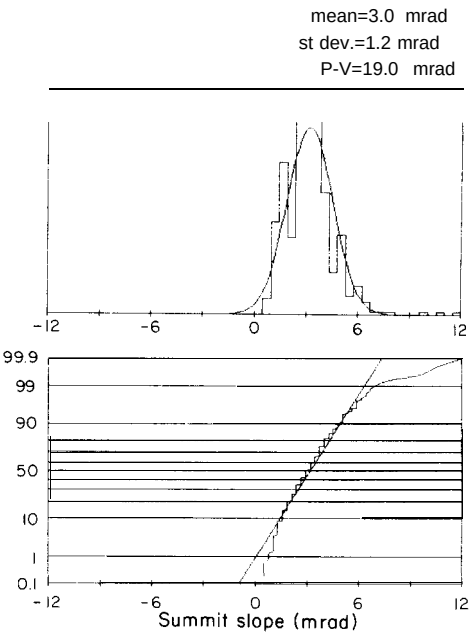

Fig. 4(*i*)

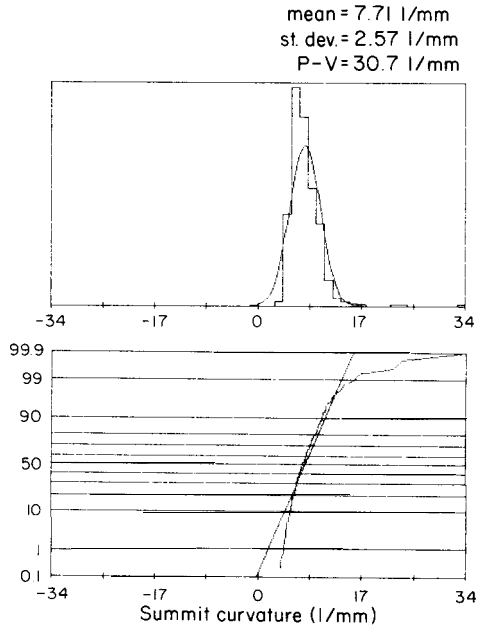

Fig. 4(i)

Fig. 4 Data for Tape AA taken at 20X. (a) Surface plot and profile in the x axis (horizontal direction is the longitudinal direction). *(b)* Histogram and distribution of surface heights. (c) Histogram and distribution of profile slope in the x axis. (d) Histogram and distribution of surface slope. (e) Histogram and distribution of profile curvature in the x axis. (f) Histogram and distribution of surface curvature. (g) Autocovariance function (horizontal direction is the longitudinal direction). (h) Histogram and distribution of summit heights. (i) Histogram and distribution of summit slopes. (j) Histogram and distribution of summit curvature.

number of surface zero crossings per length, we used the analysis of Longuet-Higgins [13]. The number of zero crossings per unit length is given by the total length of the contour where the autocovariance function is zero divided by the area enclosed by the contour.

4 Resolution, Repeatability, and Accuracy

The lateral resolution of the instrument is about 1.25 μm and 2.5 μm at 20X and 10X objective magnifications, respectively.

Table 2 Surface topography statistics of tape AA, from two-dimensional and three-dimensional profilers at objective magnifications of 10X and 20X

	3-D		2-D	
	10x	20x	10x	20x
Rms surface height, nm	19.1	12.3	11.1	12.1
Rms profile slope x, mrad	2.1	4.4	4.3	7.8
Rms profile slope y, mrad	1.8	4.2	–	–
Mean surface slope, mrad	2.4	5.3	–	–
Standard deviation surface slope, mrad	2.8	6.1	–	--
Rms profile curvature x, 1 /mm	0.99	3.97	3.83	12.66
Rms profile curvature y, l/mm	0.88	3.75	–	–
Rms surface curvature l/mm	0.71	2.82	–	–
Summit height,* nm				
Mean	10.5/ 19.2	12.7/ 21.6	6.5/ 19.3	6.2/ 20.4
Standard deviation	18.8/ 13.6	12.1/ 7.4	10.1/ 5.2	11.6/ 5.8
Summit |slope| , * mrad				
Mean	1.5/	3.1/ 3.2	1.6/ 2.3	2.4/ 2.9
Standard deviation	0.5/ 0.5	1.1/ 1.3	1.6/ 1.7	2.31 2.1
Summit curvature,* l/mm				
Mean	1.92/ 1.98	7.52/ 8.11	4.94/ 5.87	16.20/ 18.60
Standard deviation	0.59/ 0.59	2.57/ 2.97	2.32/ 2.57	7.84/ 9.00
Summit-to-valley distance, nm	140	107	88	98
Number of summits per square millimeter*	2184/ 1572	7003/ 3584	40,357/ –	21,400/ –
Profile zero crossings x, l/mm	50	78	124	104
Profile zero crossings y, l/mm	38	78	–	–
Surface zero crossings, l/mm	70	225		--
Autocorrelation distance, μm	42	21	50	40
Anisotropy ratio	5.1	3.5	–	–

*All summits/summits with top 25 percent summit height.

Table 3 Surface topography statistics from three-dimensional profiler at objective magnification of 20X

	Tape A new	Tape A worn**	Rigid disk	Floppy disk, 88.9mm Ø	Ni-Zn ferrite substr.	Silicon water	Glass slide
Rms surface height, nm	21.9	29.5	9.3	15.0	2.2	1.8	1.4
Rms profile slope x, mrad	4.2	4.4	3.6	4.1	1.3	1.7	1.1
Rms profile slope y, mrad	5.2	5.3	4.0	4.9	1.2	1.5	0.9
Mean surface slope, mrad	5.8	5.9	4.5	5.4	1.5	1.0	1.2
Standard deviation surface slope, mrad	6.7	6.9	5.3	6.3	1.8	2.3	1.4
Rms profile curvature x, l/mm	3.72	4.11	3.76	4.07	1.88	2.39	1.59
Rms profile curvature y, l/mm	4.44	4.56	4.12	4.42	1.67	2.11	1.27
Rms surface curvature, l/mm	3.12	3.32	2.89	3.22	1.41	1.92	1.14
Summit height, * nm							
Mean	12.1/ 23.8	13.9/ 24.7	9.6/ 15.1	9.9/ 15.8	3.1/ 4.3	3.1/ 4.6	3.4/ 4.3
Standard deviation	22.2/ 15.4	28.4/ 20.1	8.7/ 5.3	15.1/ 12.7	2.5/ 2.2	1.5/ 0.9	2.2/ 1.9
Summit |slope|,* mrad							
Mean	3.0/ 3.0	3.4/ 3.4	3.3/ 3.6	3.4/ 1.1	2.0 2.1	2.1 2.3	1.9 2.1
Standard deviation	1.2/ 1.2/	1.1/ 1.3/	1.1/ 1.3/	1.1/ 1.1/	0.7/ 0.8	0.5/ 0.7	0.7/ 0.7
Summit curvature,* l/mm							
Mean	7.71/ 7.91/	8.11/ 8.30/	8.11/ 8.70	8.30/ 8.50	4.94/ 5.14	5.14/ 5.54	4.75/ 4.94
Standard deviation	2.57/ 2.77/	2.97/ 3.16	2.97/ 3.16	2.77/ 2.97	1.58/ 1.78	1.19/ 1.38	1.38/ 1.58
Summit-to-valley distance, nm	180	223	142	241	35	62	28
Number of summits per square millimeter*	6543/ 4413	8074/ 5230	11,071/ 6480	10,089/ 7577	3227/ 2181	10,816/ 4783	753/ 485
Profile zero crossings x, l/mm	29	35	46	35	57	71	43
Profile zero crossings y, l/mm	54	46	68	93	67	50	75
Surface zero crossings, l/mm	127	106	235	190	370	565	467
Autocorrelation distance, μm	40	32	14	13	35	41	19
Anisotropy ratio	2.8	3.1	1.3	1.3	1.5	3.4	1.2

*All summits/summits with top 25 percent summit height.
**For 5000 file passes.

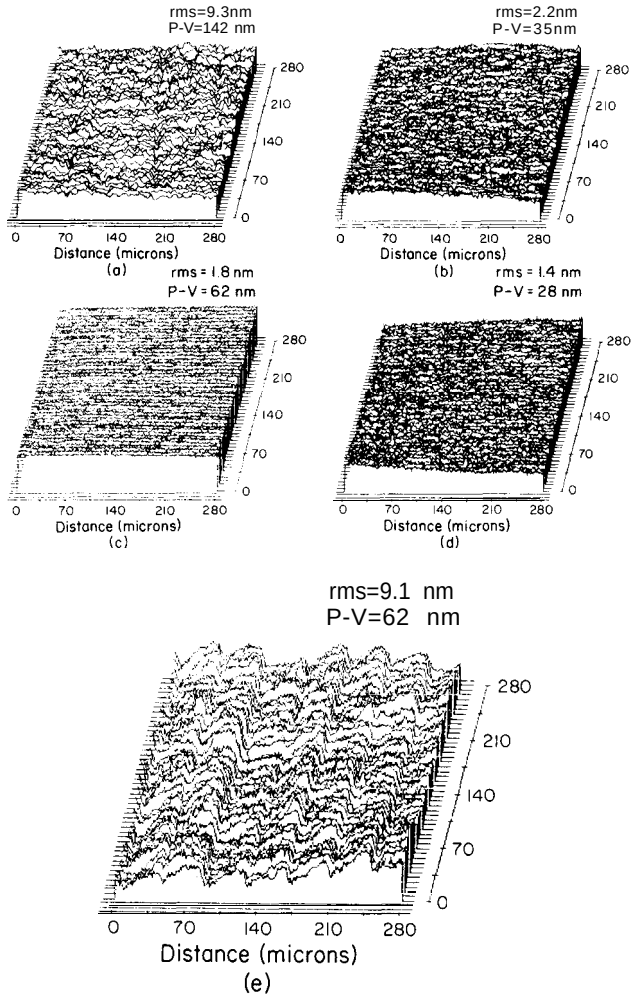

Fig. 5 Surface plots. (a) Rigid disk, radial direction along horizontal axis. (b) Lapped Ni-Zn ferrite. (c) Silicon wafer. (d) Glass slide. (e) Diamond-turned aluminum circular substrate for rigid disk, radial direction along horizontal axis.

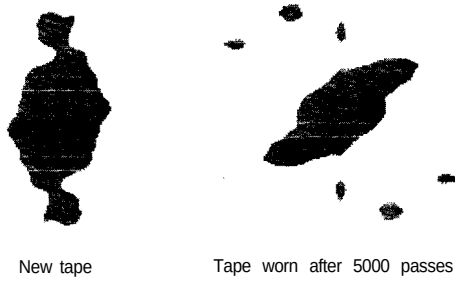

Fig. 6 Plot showing the points for which the autocovariance is greater than 0.1. The longitudinal direction of the tape is along the horizontal direction.

The repeatability of the measurements depends upon surface reflectivity and surface roughness. Our experience indicates that the repeatability for typical magnetic tapes is approximately 0.5 to 1 nm rms.

To determine the accuracy of the instrument, we made a measurement on a calibration standard for a stylus profiler (Fig. 3). A step 46 nm deep was measured to be 45.5 nm. Therefore, the accuracy of the instrument is within 1 nm.

5 Results and Discussion

The profiler can be used at an objective magnification of either 10X or 20X. Measurements were made on a computer tape AA, at both magnifications, and the results were compared with measurements of the same tape using a two-dimensional optical profiler [2]. Results are presented in Table 2. Note that the measured values using the linear array

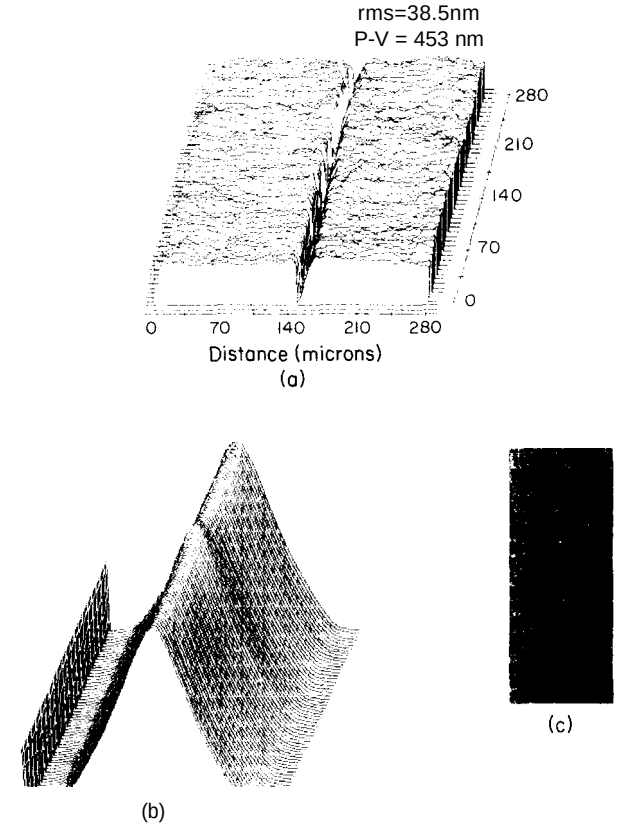

Fig. 7 Example of wear scratch on the tape surface (the longitudinal direction of the tape is along the vertical direction). (a) Surface plot.(b) Autocovariance function. (c) Contour for which autocovariance is greater than 0.1.

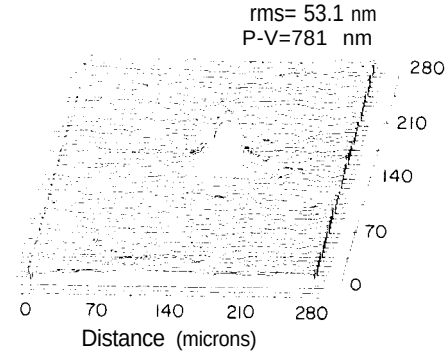

Fig. 6 Surface plot of high asperity present on Tape A

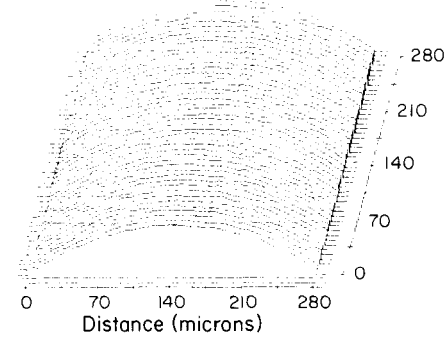

Fig. 9 Surface plot of a magnetic head with a cylindrical contour radius of 20 mm

at 10X are comparable to those of the two-dimensional array at 20X because pixel spacings in three dimensions (1.25 μm) are comparable to those in two dimensions (1.3 μm). Values at different magnifications differ for each array because of the difference in pixel spacing [2].

The sample plots for a typical computer tape A[1], taken at 20X, are shown in Fig. 4. Because plots of profile slopes and curvatures along they axis are comparable to those along the x axis, plots along they axis are not presented in Fig. 4. Note that surface heights, profile slopes in the x and y directions, profile curvatures in the x and y directions, and surface curvature are Gaussian [l]. The surface slope is not expected to be Gaussian, but all the summit heights are nearly Gaussian. However, the summit heights for summits with upper 25 percent heights, the slopes and curvatures for all summits, and the slopes and curvatures for summits with upper 25 percent heights are not Gaussian [l]. We have also found that worn tape surfaces depart from a Gaussian distribution.

Table 3 shows typical data of tape A (both new and after 5000 full file passes), a rigid disk, a floppy disk (88.9-mm diameter), a lapped Ni-Zn ferrite substrate, a silicon wafer, and a glass slide. Typical three-dimensional plots are shown in Fig. 5. From Table 3, we note that the anisotropy ratio is very high for tapes, compared to other substrates. Rigid and floppy disks are burnished, which provides a random surface roughness; lapping of silicon and Ni-Zn ferrite also provides a random roughness; tape, however, is calendered in the longitudinal direction and is expected to be anisotropic. The anisotropy ratio and autocorrelation distance are useful parameters for monitoring a manufacturing process or comparing different processes.

Figure 6 shows the contour plot of new and worn samples of tape A where the autocovariance function is greater than 0.1. Note that the wear causes a rotation of the contour. Because tape wear might result in longitudinal scratches, we expect the autocorrelation distance to increase in the longitudinal direction, which would result in the rotation seen in the figure. Figure 7 shows an example of a surface scratch on the tape after wear. Note that the autocovariance function becomes anisotropic with a very large autocorrelation distance along the scratch, as expected. Figure 8 shows an example of the high asperity present on a tape surface. Figure 9 shows an example of a surface profile of a head contour.

[1] Tape A and tape AA are the same in composition, but differences in calendering temperature and pressure result in different surface roughnesses.

6 Conclusions

A three-dimensional, noncontact, digital, optical profiler has been successfully developed using Mirau interferometry and a 384 x 244 pixel CID image sensor. The lateral resolution of the instrument is about 2.5 μm and 1.25 μm at objective magnifications of 10X and 20X, respectively. The repeatability of the instrument is on the order of 0.5 to 1 nm rms. Accuracy is better than 1 nm. Areas of 0.56 x 0.56 mm and 0.28 x 0.28 mm are measured at objective magnifications of 10X and 20X, respectively.

References

1 Wyant, J. C., Koliopoulos, C. L., Bhushan, B., and George, O. E., "An Optical Profilometer for Surface Characterization of Magnetic Media," ASLE *Trans.*, Vol. 27, Apr. 1984, pp. 101-113.

2 Bhushan, B., Wyant, J. C., and Koliopoulos, C. I.., "Measurement of Surface Topography of Magnetic Tapes by Mirau Interferometry." *Appl. Opt.*, Vol. 24, May 1985, pp. 1489-1497.

3 Young, R., Ward, J., and Scire, F., "The Topografiner: An Instrument for Measuring Surface Microtopography," *Rev. Sci. Instr.*, Vol. 43, July 1972, pp. 999-1011.

4 Gassel, S. S., SKF Industries, Inc., Private communication regarding three-dimensional microscale topography system-stereoscopic image pairs generated by an SEM, 1981.

5 Uchida, S., Sato, H., and O-Hori, M., "Two-Dimensional Measurement of Surface Roughness by the Light Sectioning Method," *Ann. CIRP*, Vol. 28, *1979*, pp. 419-423.

6 Sato, H., and O-Hori, M., "Surface Roughness Measurement by Scanning Electron Microscope," *Ann. CIRP*, Vol. 31, pp. 457-462, 1982.

7 Perry, D. M., Moran, P. J., and Robinson, G. M., "Three-Dimensional Surface Metrology of Magnetic Recording Materials Through Direct Phase Detecting Microscopic Interferometry," *Proc. Fifth Conf. on Video and Data Recording*, University of Southampton, Apr. 1984.

8 Tsukada, T., and Sasajima, K., "A Three-Dimensional Measuring Technique for Surface Asperities," Wear, Vol. 71 1981, pp. l-14.

9 Giaever, I., "Energy Gap in Superconductors Measured by Electron Tunnelline." *Phys. Rev. Lett.*, Vol. 5, 1960, pp. 147-148.

10 Binnig, G., and Rohrer, H., "Scanning Tunnelling Microscopy," *Surface Sci.*, Vol. 126, 1983, pp. 236-244.

11 Golovchenko, J. A., "Studies of Metal and Semiconductor Surfaces with the Scanning Tunnelling Microscope," presented at American Physical Society Meeting, Baltimore, Md., Mar. 25-29, 1985.

12 Nayak, P. R., "Random Process Model of Rough Surfaces," ASME *Journal of Lubrication Technology*, Vol. 93, 1971, pp. 398-407.

13 Longuet-Higgins, M. S., "The Statistical Analysis of a Random, Moving Surface," *Phil. Trans. R. Soc.*, Vol. 249, Ser. A, 1957, pp. 321-387.